Environmental Science & Technology

pubs.acs.org/est

Article

Enhancing Sediment Bioaccumulation Predictions: Isotopically Modified Bioassay and Biodynamic Modeling for Nickel Assessment

Qijing Su, Wenze Xiao, Stuart L. Simpson, Qiao-Guo Tan, Rong Chen, and Minwei Xie*

Cite This: *Environ. Sci. Technol.* 2023, 57, 19352−19362

Read Online

ACCESS | Metrics & More | Article Recommendations | Supporting Information

ABSTRACT: Quantifying metal bioaccumulation in a sedimentary environment is a valuable line of evidence when evaluating the ecological risks associated with metal-contaminated sediments. However, the precision of bioaccumulation predictions has been hindered by the challenges in accurately modeling metal influx processes. This study focuses on nickel bioaccumulation from sediment and introduces an innovative approach using the isotopically modified bioassay to directly measure nickel assimilation rates in sediment. Tested in sediments spiked with two distinct nickel concentrations, the measured Ni assimilation rates ranged from 35 to 78 ng g^{-1} h^{-1} in the Low-Ni treatment and from 96 to 320 ng g^{-1} h^{-1} in the High-Ni treatment. Integrating these rates into a biodynamic model yielded predictions of nickel bioaccumulation closely matching the measured results, demonstrating high accuracy with predictions within a factor of 3 for the Low-Ni treatment and within a factor of 1 for the High-Ni treatment. By eliminating the need to model metal uptake from various sources, this streamlined approach provides a reliable method for predicting nickel bioaccumulation in contaminated sediments. This advancement holds promise for linking bioaccumulation with metal toxicity risks in sedimentary environments, enhancing our understanding of metal-contaminated sediment risks and providing valuable insights to support informed decision-making in ecological risk assessment and management.

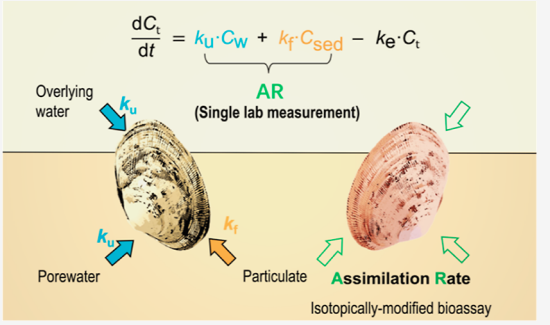

KEYWORDS: *metal-contaminated sediments, bioavailability, biodynamic modeling, ecological risk assessment, Ruditapes philippinarum*

1. INTRODUCTION

Metal bioaccumulation is an integrative measure of the accumulation of metal contaminants in organism tissue across various sources over a specific time frame.[1] Tissue metal concentrations in biomonitor organisms indicate the locations of bioavailable metal exposure[2−4] and can be viewed as the initial step in the cascade of toxicity processes.[5−7] However, metal bioaccumulation data have been of limited utility in assessing the associated ecological risks and have thus been underutilized in regulatory applications, especially in the management of contaminated sediments.[2,8,9] The limited practicality of utilizing metal bioaccumulation data for risk assessment stems from the organism's intricate processes of internally regulating metal concentrations that partition accumulated metals into separate metabolically available and biologically detoxified forms.[6,7,10]

Biodynamic modeling is a biologically based conceptual model, aiming to quantitatively predict the net bioaccumulation by considering metal influx and efflux processes.[2,5] This modeling approach utilizes a set of rate expressions to mathematically unify the key processes, such as the uptake of dissolved metals, the dietary uptake of metals (i.e., ingestion of food or sediment particulates), the loss of metals, and the growth dilution of tissue metal concentrations. Through carefully designed experiments, it becomes possible to quantify these physiological processes and derive key physiological constants. By utilizing these relationships, the models enable predictions of bioaccumulation, thereby establishing a link between metal exposure and bioaccumulation across diverse environmental conditions.

While biodynamic bioaccumulation models have shown success in identifying exposure pathways and physiological processes that govern metal bioavailability and inform risk assessment in aquatic environments,[5,11−13] their application becomes increasingly complex in sedimentary settings.[14] In sediments, organisms can directly uptake metals through sediment ingestion, adding to metal uptake through aqueous pathways (overlying water and porewater).[15,16] However, establishing a clear link between bioavailability, as inferred from bioaccumulation, and sediment concentration has proven to be a challenging task. The bioavailable fraction of metals in sediments is intricately controlled by factors such as metal speciation, which is significantly affected by the redox

Received: July 24, 2023
Revised: October 27, 2023
Accepted: October 30, 2023
Published: November 16, 2023

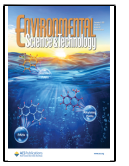

condition, sediment matrix composition, sediment heterogeneity, and the dynamics of ambient environmental conditions.[14,17,18] Additionally, dietary accumulation is influenced by the rate of sediment ingestion by organisms and their efficiency in assimilating metals from sediments.[19−21] These complexities present substantial obstacles when attempting to apply biodynamic modeling to sediments, particularly when aiming to establish a direct connection among metal exposure, bioaccumulation, and the prediction of ecological risks.[14]

Recently, Croteau et al. introduced an innovative reverse-labeling method for evaluating the individual bioavailability of copper[22] and zinc[23] on natural particles in aquatic environments. Building upon this concept, we have tailored a simplified approach known as the isotopically modified bioassay to concurrently assess the bioavailability of multiple metals within contaminated sediment matrices.[24,25] This approach involves modifying the isotopic composition of metals in an organism and then exposing them to a metal-contaminated sediment. The uptake of metals induces a measurable change in the isotopic composition, which can be quantified through calculation. We have successfully applied this approach to assess changes in metal bioavailability during sediment resuspension[24] and to determine metal bioavailability in deposited sediments.[25] In the latter study, we identified a bioavailability-relevant parameter known as the metal assimilation rate, which quantifies the mass of metal uptake per unit of organism weight over a specific exposure period. This "assimilation rate" parameter describes the net rate at which metals are absorbed by the organism during sediment exposure, encompassing exposure through overlying water, porewater, and sediment pathways. Notably, this expression shows promise as a direct replacement for the various rate expressions of metal influx in the biodynamic model. By incorporating the metal assimilation rate, the need to separately consider the contributions of metal uptake through individual pathways can be minimized, thereby simplifying the modeling process.

Accordingly, the primary objective of the study was to assess the feasibility of using the isotopically modified bioassay for rapid metal bioavailability measurements to predict long-term metal bioaccumulation within a biodynamic modeling framework. To achieve this, both the isotopically modified bioassay and the long-term bioaccumulation bioassay were deployed in the same sedimentary environment. Metal assimilation rates from the rapid bioassay were used to model longer-term nickel accumulation in clams exposed to the same environment.

2. MATERIALS AND METHODS

2.1. Water, Organisms, and Ni-Treated Sediments. Clean seawater with a salinity of 32 was collected from the Xiamen Bay (24°25′26″ N, 118°8′18″ E), Xiamen, China. Before being used in the experiment, the seawater was filtered through a membrane filter (mixed cellulose ester membrane) with a pore size of 0.22 μm and adjusted to a salinity of 25 by adding deionized water (Milli-Q, 18 MΩ·cm).

A benthic filter-feeding clam species that burrows shallowly in the sediments (*Ruditapes philippinarum*) was tested in the bioaccumulation experiment.[26,27] This species is widely distributed along the coast of China.[28] The clams, with a shell length of 1.9−2.5 cm, were collected in the lower intertidal region under the Jimei Bridge of Xiamen City (24° 33′32″ N, 118° 8′31″ E). These clams were then acclimated in the clean seawater (salinity 25) in the laboratory (21 ± 1 °C, 14 h: 10 h of light/dark cycle) for a week before being used, during which they were fed the green algae *Chlorella* sp. (3.5 mg clam^{-1}) daily.

Clean sediment was collected from Qiongtou Bay (24°39′48″ N, 118°11′12″ E), Xiamen, China. Surficial sediments (0−5 cm depth) were press-sieved through a stainless-steel mesh sieve (2 mm pore size) in the field to remove large debris (rock and shells). The sieved sediments were placed into a 20 L plastic bucket with no free headspace, sealed, transported back to the laboratory, and stored at room temperature (21 ± 1 °C).

This study focuses on examining the bioaccumulation of nickel (Ni) in estuarine/marine sediment. This topic was chosen due to growing environmental concerns regarding the presence of elevated nickel in the estuarine and marine environments,[29,30] particularly within the global context of extracting nickel from surface-enriched nickel laterite deposits.[31] These large-scale open-cast mining operations predominantly occur along tropical coastlines, leading to elevated nickel concentrations in estuarine sediments.[31−33]

While it would be feasible to employ naturally contaminated sediments for our research purpose, we did not have access to nickel-contaminated sediments that were not cocontaminated with relatively high concentrations of other metals and low concentrations of polyaromatic hydrocarbons (PAHs). Therefore, we chose to create a laboratory-spiked sediment that was primarily contaminated by nickel.

The generation of nickel-contaminated sediments encompassed the spiking of nickel chloride solution into clean sediment, followed by a five-month equilibration.[29,34] Briefly, an initial stock Ni-contaminated sediment (referred to as superspike sediment) with a nickel concentration of 20,000 mg Ni kg^{-1} wet weight was first prepared in a N_2-filled glovebox to minimize oxidation processes by adding 500 mL of nickel chloride solution (80 g L^{-1}, chemical dissolved in deoxygenated seawater) to 2 kg of clean wet sediment. The sediment−water mixture underwent thorough mixing via end-to-end rotation in a sealed bottle for 1 day, with a frequency of 100 oscillations per min using a variable speed multipurpose oscillator (Guohua Electric Appliances Co., Ltd.). Throughout this process, the pH of the sediment slurry experienced a moderate decrease, periodically necessitating adjustments and returned back to a neutral value of 7 upon supplementing with 4 mol L^{-1} NaOH. Subsequently, the superspike sediment was left to equilibrate at room temperature for 5 months, during which the pH of the sediment was monitored and adjusted when necessary in the initial weeks until the pH was stabilized.

Nickel concentrations in estuarine sediments worldwide are typically <100 mg kg^{-1}[35,36] but can be as high as 7700 mg kg^{-1} in regions significantly contaminated.[32] Accordingly, two different nickel concentrations were tested in the bioaccumulation experiment: a low-Ni sediment of 200 mg of Ni kg^{-1} dry weight and a high-Ni sediment of 2000 mg of Ni kg^{-1} dry weight. These concentrations, respectively, mirror sediments with moderate and high nickel contamination levels. The preparation of these treatments involved diluting the rehomogenized "superspike sediment" with the clean sediment to achieve the intended nominal concentrations.[37] After the dilution process, both sediments were allowed to equilibrate for a period of 5 days before the commencement of the bioaccumulation experiment.

2.2. Experimental Setup for Sedimentary Bioaccumulation Test. The exposure of clams to contaminated

https://doi.org/10.1021/acs.est.3c05914
Environ. Sci. Technol. 2023, 57, 19352−19362

sediments was conducted using eight plastic chambers (30 cm in length, 19.5 cm in width, and 17 cm in height). Each of the two experimental conditions (low-Ni and high-Ni treatments) was subjected to four replicates. Within each plastic chamber, Ni-contaminated sediments were introduced to provide a sediment depth of 3.5 cm. Subsequently, clean seawater was gently introduced to form a 10 cm water column over the sediment. Continuous aeration of overlying seawater was achieved using aquarium stones with adjustment of the air supply rate to ensure effective water mixing without inducing suspension of sediment particles.

Throughout the experimental duration, introduction and retrieval of clams were performed at regular intervals (detailed in Section 2.4). To facilitate the retrieval of clams that had burrowed within the sediment, the experimental system was improved on the second day of commencement by placing a plastic mesh (1.5 mm pore size) at a depth of 1 cm within the sediment. The positioning of the mesh served a dual purpose: it guided clam activity within the near-surface layer of sediments (within the upper 1 cm) for efficient retrieval while still allowing the clams to maintain their natural burrowing behavior within the sediment.

The plastic mesh, measuring 30 cm in length and 19.5 cm in width, featured a square opening in one corner of the chamber. This opening was specifically designed to facilitate the deployment of the diffusive gradients in thin-film (DGT) device.[38,39]

2.3. Preparation of the Isotopically Modified Bioassay for Rapid Determination of Metal Bioavailability in Sediment. To assess the bioavailability of metals in sediments over a short time frame, an isotopically modified bioassay technique[24,25] was used, consisting of two primary stages. In the initial isotopic-modification stage, the bioassay utilized a stable metal isotope to modify the isotopic composition of the clam tissue. Subsequently, the bioassay underwent a contaminant exposure stage, where it was exposed to metal-contaminated sediments. The quantification of metal bioavailability in sediments was achieved by analyzing the shifts in the metal isotopic composition within the clam tissue.

During the initial isotopic-modification stage, the clams were cultured in Ni^{62}-spiked seawater (5 $\mu g\ L^{-1}$, Ni^{62} isotope purchased from ISOFLEX, San Francisco, California, 99.36% purity) for 14 days to enhance Ni^{62} abundance in clam tissue. To accommodate the six time intervals of the deployment of isotopically modified bioassay throughout sedimentary bioaccumulation test (Section 2.4), six separate bioassay batches were created, each starting its culturing process 14 days before the sediment deployment.

To ensure consistent isotope enrichment efficiency among and within batches, a flow-through culture system was used. 110 clams were cultured in 6.6 L of Ni^{62}-spiked seawater (about 60 mL per clam) in a 20 L plastic container. The seawater was consistently renewed with fresh Ni^{62}-spiked seawater at 4.6 mL min^{-1} (1 day turnover). During this 14 day enrichment, the clams were fed daily with Chlorella sp. (3.5 mg $clam^{-1}$) for 1 h in a separate container, rinsed, and returned to the system. To evaluate the isotopic composition changes, ten clams from each batch were sampled on the first and final days of the culture.

In the subsequent sediment exposure stage, isotopically modified clams were introduced into the sediment exposure chamber at various time intervals, as per Section 2.4. After the designated period of sediment exposure, the clams were retrieved, rinsed, and underwent an 8 h depuration in seawater amended with 1 mM ethylenediaminetetraacetic acid (EDTA). The depuration period was predetermined to enable complete evacuation of gut-retained sediments. The EDTA addition aimed to counter any potential additional nickel uptake from natural seawater (at trace levels, 2.7 ± 0.6 $\mu g\ L^{-1}$). A preliminary test, investigating the impact of EDTA addition on the efflux of metals in another estuarine clam species (*Potamocorbula laevis*, data not shown), confirmed that nickel efflux from the organism in the presence of 1 mM EDTA remained unaffected. During depuration, the clams were not fed, and the seawater was renewed when fecal matter was observed. Subsequently, the clams were sampled for the nickel isotopic analysis.

2.4. Experimental Procedures for Sedimentary Bioaccumulation Test. Sedimentary bioaccumulation test was designed to assess the potential of using isotopically modified bioassay measurement (1 or 3 days of exposure) to predict long-term metal bioaccumulation (18 days) in sediment. This involved introducing both isotopically modified clams (for short-term bioaccumulation assessment) and unmodified clams (for long-term bioaccumulation, tagged for differentiation, Figure S1, Supporting Information) into a common sediment exposure chamber under uniform conditions.

One day prior to the experiment, eight plastic chambers were filled with homogenized sediments (3.5 cm of depth) and clean seawater (10 cm water column). The sediment−water system was stabilized for 24 h.

On the first day of the test (Day 0), the overlying water was drained to a depth of 1 cm. The tagged unmodified clams (Figure S1) and the isotopically modified clams were evenly distributed on sediment surface (burrowed within 1 h). The seawater was then replenished to its original depth. The bioaccumulation test was then started and lasted 18 days with periodic introduction and retrieval of organisms, DGT devices, and water sampling.

The frequency of adding and retrieving unmodified clams (for the long-term bioaccumulation bioassay) varied slightly between treatments: in the low-Ni treatment, 10 clams were added on Day 0 and retrieved on Days 9 (5 clams) and 18 (5 clams), while in the high-Ni treatment, 10 clams were added on Day 0 and retrieved solely on Day 18.

For the isotopically modified bioassay, the addition and retrieval occurred on a 3 d cycle basis. In the low-Ni treatment, 4 isotopically modified clams were added on Days 0, 3, 6, 9, 12, and 15, and retrieved on the following day (24 h exposure). In contrast, in the high-Ni treatment, 7 isotopically modified clams were added on Days 0, 3, 6, 9, 12, and 15. These clams were then retrieved after 1 day (24 h) exposure (3 clams on Days 1, 4, 7, 10, 13, and 16) and 3 day (72 h) exposure (4 clams on Day 3, 6, 9, 12, 15, and 18), respectively. The varied exposure duration approach was intentionally designed to explore the potential differences in bioavailability measurements arising from the exposure durations with the understanding that any disparities would be more readily discernible in the high-Ni treatment.

Commercially available piston-type Chelex-DGT devices (purchased from DGT Research Ltd.) were deployed in both treatment scenarios alongside the 1 day exposure isotopically modified bioassay. On Days 0, 3, 6, 9, 12, 15, and 18, deoxygenated DGT devices[40] were inserted vertically into the sediment until their upper rim aligned with the sediment−water interface (SWI), positioning the entire active metal-

https://doi.org/10.1021/acs.est.3c05914
Environ. Sci. Technol. 2023, 57, 19352−19362

binding surface of the devices within the sediment. This allowed them to capture the measurements of "DGT-labile" metals at a depth of 0.5−2.5 cm below the SWI (exposure area = 3.14 cm^2) (as detailed in Note S1, Supporting Information). Following a 24 h deployment, the DGT devices were carefully retrieved to minimize disturbance to the sediment structure, with the notches created by their removal being gently refilled with ambient sediment.

The overlying water was renewed on Days 1, 4, 7, 10, 13, and 16, aligning with the retrieval of organism and DGT device. To minimize sediment resuspension, a specific procedure was followed: the overlying water was first drained to a depth of approximately 1 cm, followed by sampling of organisms and DGT devices, and subsequently, clean seawater was then added to restore it to the original depth. An additional water renewal occurred on Day 9 in the low-Ni treatment when unmodified clams were retrieved.

2.5. Sampling and Analysis. Comprehensive details regarding the sampling and analysis of sediments, waters, clams, and DGTs can be found in Note S2, Supporting Information. Here, we provide a succinct overview of the primary procedures.

The sediments were characterized for particle size distribution, dilute-acid (1 M HCl) extractable metal (AEM)[9] and total recoverable metal (TRM)[41] concentrations.

During the bioaccumulation experiment, overlying seawater was sampled on Days 0, 1, 3, 4, 6, 7, 9, 10, 12, 13, 15, 16, and 18, both before and after the water renewal. The water (10 mL) was filtered (PES membrane filter, 0.45 μm pore size), acidified (pH < 1), and stored for metal analysis.

The clams were retrieved and immediately processed, including dissection, freeze-drying of soft tissue, and digestion in 65% HNO_3 at 80 °C for 8 h. Diluted acid digest solution (~2% HNO_3) was then analyzed for metal isotope concentrations.

Within 40 days of DGT retrieval, deployed and blank DGT samplers were disassembled. The metal-binding layer for each sampler was digested in 1 mL of 1 M HNO_3 for 24 h. The eluent was then diluted and determined for Fe, Mn, and Ni concentrations.

Metal concentrations in water and acid digest were determined using inductively coupled plasma−mass spectrometry (ICP−MS, NexION 2000, PerkinElmer). Ni^{60} and Ni^{62} were analyzed for nickel, and Mn and Fe concentrations were also determined in water and the DGT eluent samples. Detailed information on quality assurance and quality control procedures can be found in Note S2, Supporting Information.

2.6. Analyzing Isotopic Data to Determine Nickel Assimilation Rate from the Sediment. *2.6.1. Newly Accumulated Concentration of Ni^{62} in the Clams.* During the isotopic-modification stage, the clams were cultured in Ni^{62}-spiked seawater. The increase in Ni^{62} concentration in clam tissue ($Ni^{62}|_{new}$, $\mu g\ g^{-1}$ dry weight) can be calculated using the following equation[25]

$$Ni^{62}|_{new} = (Ni^{62}|_{meas} - Ni^{60}|_{meas}) \times 0.0363 \quad (1)$$

where $Ni^{62}|_{meas}$ and $Ni^{60}|_{meas}$ ($\mu g\ g^{-1}$) are the instrument-reported Ni concentrations obtained by analyzing the Ni^{62} and Ni^{60} isotopes in the sample, respectively. The value of 0.0363 represents the natural isotope abundance of Ni^{62}. When measuring nickel concentrations, the ICP−MS instrument assumes that the sample has the same isotopic composition as that of the calibration standards (i.e., natural abundance). Due to clams absorbing purely Ni^{62} from seawater during the culture, the instrument reported a higher total Ni concentration than the actual value by analyzing the Ni^{62} isotope. In contrast, the instrument reported a lower total Ni concentration than the actual value upon analysis of the Ni^{60} isotope. The actual accumulated Ni^{62} concentration can thus be calculated from the difference of the two reported concentrations using eq 1. For a more detailed explanation and further details regarding this calculation, please refer to our previous publications.[24,25]

2.6.2. Nickel Assimilation Rate Determination following Sediment Exposure. The accumulation of Ni^{62} during the isotopic-modification stage caused an increase in the Ni^{62} to Ni^{60} ratio ($Ni^{62/60}$).[24,25] This ratio was calculated using the equation

$$Ni^{62/60} = \frac{Ni^{62}|_{meas} \times 0.0363}{Ni^{60}|_{meas} \times 0.262} \quad (2)$$

where the value of 0.262 is the natural isotope abundance of Ni^{60}.

When exposed to Ni in sediments, the clams absorbed both isotopes at their natural abundances, leading to a corresponding decrease in the $Ni^{62/60}$ ratio. The isotopic ratio in clams exposed to sediment was calculated using the equation

$$Ni^{62/60}|_{exp} = \frac{Ni^{62}|_{meas|exp} \times 0.0363}{Ni^{60}|_{meas|exp} \times 0.262} \quad (3)$$

In our previous study, we established a baseline condition by placing a reference group of clams in clean water for the same duration as the sediment-exposed clams.[25] We determined the isotopic ratio in these clams, which were not exposed to Ni-contaminated sediment. However, we found this step unnecessary, as using the isotopic composition of clams at the final day of the isotopic modification stage as the baseline did not compromise the analysis quality (i.e., yielding similar results). Thus, we calculate the baseline isotopic ratio using the following equation

$$Ni^{62/60}|_{base} = \frac{Ni^{62}|_{meas|base} \times 0.0363}{Ni^{60}|_{meas|base} \times 0.262} \quad (4)$$

where $Ni^{62}|_{meas|base}$ and $Ni^{60}|_{meas|base}$ were determined in clams from the final day of the isotopic-modification stage.

By comparing the $Ni^{62/60}$ ratio between the sediment exposure treatment and the baseline group, we can calculate the mass of Ni (M_{Ni}, μg) absorbed based on the extent of the ratio decrease (eqs 5 and 6).[25]

$$Ni^{62/60}|_{base} = \frac{W \times Ni^{62}|_{meas|exp} \times 0.0363 - M_{Ni} \times 0.0363}{W \times Ni^{60}|_{meas|exp} \times 0.262 - M_{Ni} \times 0.262} \quad (5)$$

$$M_{Ni} = W \times \frac{Ni^{62/60}|_{base} \times Ni^{60}|_{meas|exp} \times 0.262 - Ni^{62}|_{meas|exp} \times 0.0363}{Ni^{62/60}|_{base} \times 0.262 - 0.0363} \quad (6)$$

Consequently, the total assimilation rate of Ni (AR_{Ni}, $\mu g\ g^{-1}\ d^{-1}$ or $ng\ g^{-1}\ h^{-1}$) during sediment exposure, was determined using the equation

https://doi.org/10.1021/acs.est.3c05914
Environ. Sci. Technol. 2023, 57, 19352−19362

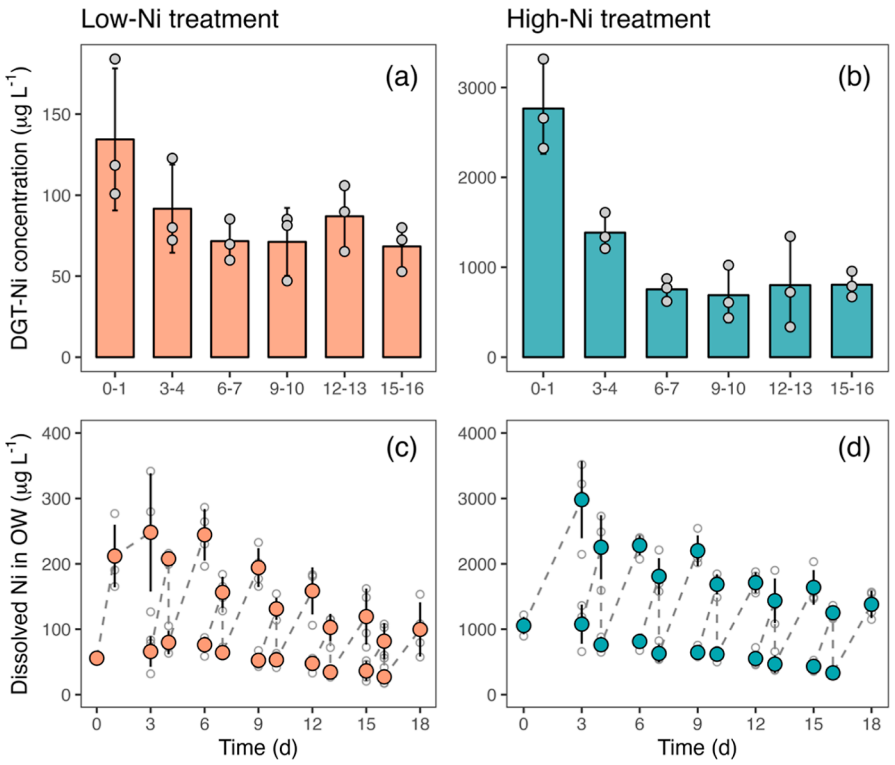

Figure 1. Variation of DGT-labile Ni concentration in sediments (a,b) and dissolved Ni concentrations in overlying water (c,d). In (a,b), each gray point represents a DGT measurement in a replicate chamber (DGT was deployed in three chambers at each time interval). The height of the column and the error bar represent the mean concentration and the standard deviation of the three replicate measurements, respectively. In (c,d), each open circle represents a dissolved nickel measurement in each chamber. The solid points and the error bar represent the mean and the standard deviation of the four replicate measurements, respectively.

$$AR_{Ni} = \frac{M_{Ni}}{W \times t_{exp}} \quad (7)$$

where t_{exp} represents the duration of sediment exposure and W is the dry weight of the clam tissue.

2.7. Incorporating the Nickel Assimilation Rate into a Biodynamic Model to Predict Long-Term Nickel Bioaccumulation. The nickel concentration in organism tissue is controlled by the balance between nickel influx and efflux, described by a biodynamic model[5]

$$\frac{dC(t)}{dt} = J_{in}(t) - J_e(t) \quad (8)$$

where $C(t)$ represents the tissue nickel concentration ($\mu g\ g^{-1}$), $J_{in}(t)$ is the influx rate ($\mu g\ g^{-1}\ d^{-1}$), and $J_e(t)$ is the efflux rate ($\mu g\ g^{-1}\ d^{-1}$).

The efflux rate J_e is defined by a proportional efflux rate constant (k_e', d^{-1}) multiplied by the tissue nickel concentration

$$J_e(t) = k_e' \cdot C(t) \quad (9)$$

We assume that the same efflux rate constant applies to clams in both sediments and water as the unidirectional metal loss is often considered specific to each organism species.[5] The determination of the efflux rate constant k_e' in water was conducted separately through an aqueous exposure-depuration test (Table S1), with detailed descriptions provided in Note S3 of the Supporting Information.

In a typical biodynamic model, metal influx derivation is a more intricate process that considers contributions from various exposure sources.[5] Instead of explicitly delineating the contribution of nickel uptake through different pathways, we incorporated the assimilation rate AR_{Ni} from the isotopically modified bioassay as the metal influx rate (eq 10).

$$J_{in}(t) = AR_{Ni} \quad (10)$$

Although the nickel assimilation rate of the isotopically modified bioassay essentially represents a net influx rate, we believe it is necessary to include a nickel efflux term in the model (eqs 8 and 9). This is because metal efflux is a proportional loss, and it may become more significant in long-term bioaccumulation bioassays at higher tissue nickel concentrations during the later stage of exposure. In contrast, the isotopically modified bioassay exhibits lower tissue nickel concentrations.

The prediction of the nickel accumulation was achieved by solving eqs 8−10 using the measured assimilation rates and k_e'. To simulate the accumulated nickel concentration in clam tissue at various exposure times, we employed the Monte Carlo method. At each time interval, we generated a thousand random assimilation rate values based on normal distributions defined by the measured mean assimilation rates and corresponding standard deviations. For days without direct measurements, we used linear interpolation based on the random data points. However, in the 3 d high-Ni sediment exposure scenario, we assumed equal assimilation rates throughout the 3 day duration, eliminating the need for interpolation. The obtained assimilation rates were then used to solve eq 8 and calculate the accumulated nickel concentrations in the clam tissue $C(t)$. This was accomplished using the "ode()" function of the "deSolve" package in R (version 4.2.2).

https://doi.org/10.1021/acs.est.3c05914
Environ. Sci. Technol. 2023, 57, 19352−19362

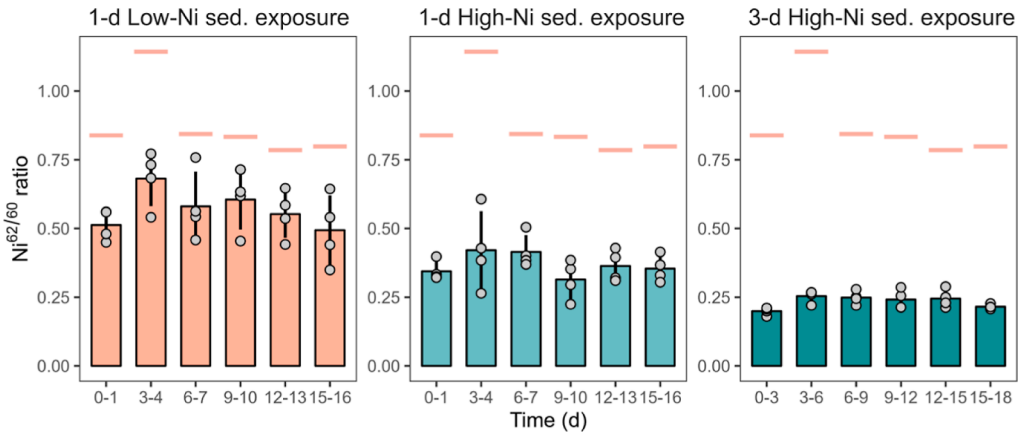

Figure 2. Variation of the $Ni^{62/60}$ ratio in clam tissue at different deployment times in different sediments. Each gray point represents the mean $Ni^{62/60}$ ratio of clams exposed in a replicate sediment chamber. The height of a column and the error bar represent the mean and the standard deviation of $Ni^{62/60}$ ratio of the four replicate treatments (corresponding to the four gray points), respectively. The orange segments represent the mean $Ni^{62/60}$ ratio of the clams in a reference treatment that were not exposed to sediment.

3. RESULTS AND DISCUSSION

3.1. Sediment Characteristics. The clean sediment used for nickel spiking was fine-grained, with 93% of the sediment being smaller than 75 μm (Table S2, Supporting Information). This sediment had very low metal concentrations, with the TRM concentrations below the corresponding sediment quality guideline values[9] (Table S2).

The two nickel-spiked sediments showed total recoverable nickel concentrations that closely matched their intended concentrations. The TRM-Ni for the sediment used in the low-Ni treatment was 260 ± 10 mg kg^{-1} (dry weight), while the sediment used for high-Ni treatment had a TRM-Ni of 2300 ± 200 mg kg^{-1} for sediment described in (Table S3). It is worth noting that a significant portion of the spiked nickel was in the reactive pool, as indicated by the high AEM-Ni/TRM-Ni ratios in the respective sediments (81% for the low-Ni treatment and 74% for the high-Ni treatment; Table S3).

3.2. Temporal Variations of Dissolved Nickel in the Overlying Water and DGT-Labile Nickel Concentrations. DGT-labile metal concentrations serve as indicators of the time-weighted average concentrations of reactive metals in the sediment. These concentrations are derived from the metals present in the porewater and labile metals that are readily released into the porewater by the sediments when the porewater metals are depleted due to the presence of the DGT sampler.

The DGT-Ni concentrations showed an order of magnitude difference between the two treatments. In the low-Ni treatment, the DGT-Ni concentrations were 87 ± 25 μg L^{-1}, whereas in the high-Ni treatment, they were 1200 ± 810 μg L^{-1} (Figure 1a,b).

Throughout the duration of the experiments, the DGT-Ni concentrations displayed an initial decrease, followed by a consistent level (Figure 1). In the low-Ni treatment, the DGT-Ni concentrations were initially higher, starting at 130 μg L^{-1} on Day 1, gradually declined to 92 μg L^{-1} on Day 4, and remained relatively constant thereafter, ranging between 68 and 87 μg L^{-1} for the remaining duration of the experiment. In contrast, in the high-Ni treatment, the DGT-Ni concentrations decreased from 2800 to 800 μg L^{-1} over the first 7 days and subsequently remained constant for the rest of the experiment (Figure 1).

The elevated nickel concentration in the sediment porewater led to the release of nickel into the overlying water. Frequent water renewal operations during the experiment decreased nickel in the overlying water. These two processes caused the observed variations of dissolved Ni in the overlying water (Figure 1c,d). In the low-Ni treatment, the dissolved nickel concentration varied between 27 and 250 μg L^{-1}, displaying a slight overall decreasing trend over time (Figure 1c). Similarly, in the high-Ni treatment, the dissolved nickel varied between 330 and 3000 μg L^{-1}, also showing a slight decreasing trend over time (Figure 1d). The nickel concentrations in the overlying water were generally greater than the DGT-labile concentrations measured in the surface sediment but generally within a factor of 2.

The concentration ranges and temporal patterns of dissolved manganese and iron in the overlying water of the two sediments showed similarities (Figure S4). In both sediments, dissolved manganese increased over the initial 3 days (from 160 to 840 μg L^{-1} in the low-Ni treatment and from 470 to 820 μg L^{-1} in the high-Ni treatment). However, following a water renewal on Day 4, the dissolved manganese concentrations decreased substantially and remained at low levels (<100 μg L^{-1}) for the rest of the experiment. In contrast, the level of dissolved iron in the overlying water remained consistently low throughout the entire duration of the experiment, ranging from 10 to 30 μg L^{-1}, and there was no significant difference between the two treatments (p = 0.71, Student's t-test).

The concentrations of the DGT labile Mn (DGT-Mn) showed similar concentration ranges and spatial variation patterns in the low-Ni and high-Ni treatments (Figure S5). In the low-Ni treatment, DGT-Mn gradually decreased from 2400 to 1200 μg L^{-1} over the course of the experiment. Similarly, in the high-Ni treatment, DGT-Mn decreased from 2400 to 1800 μg L^{-1}. In contrast, the variation magnitudes of the DGT labile iron (DGT-Fe) was different. In the low-Ni treatment, the DGT-Fe decreased from 2900 to 930 μg L^{-1} while in the high-Ni treatment, it decreased from 11,000 to 640 μg L^{-1}.

The observed similarities in manganese and iron concentrations in both the overlying water and porewater in both treatments indicate consistent geochemical conditions near the sediment−water interface where the clams were located. The only factor that differed between the treatments was the nickel

https://doi.org/10.1021/acs.est.3c05914
Environ. Sci. Technol. 2023, 57, 19352−19362

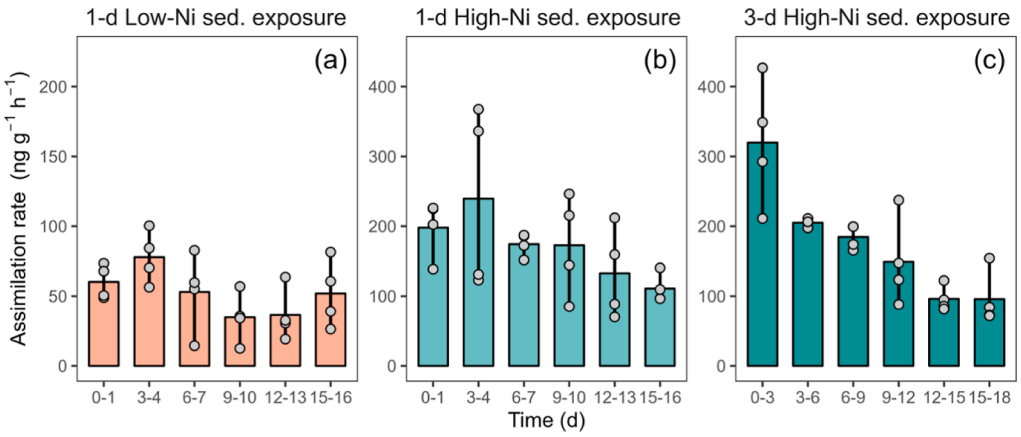

Figure 3. Nickel assimilation rates varied in different exposure scenarios in different sediments. Note that the *y*-axis scale in panel (a) is smaller than that in panel (b,c). Each gray point represents the mean assimilation rate in a replicate sediment chamber. The height of a column and the error bar represent the mean assimilation rate and the standard deviation of the four replicate treatments, respectively.

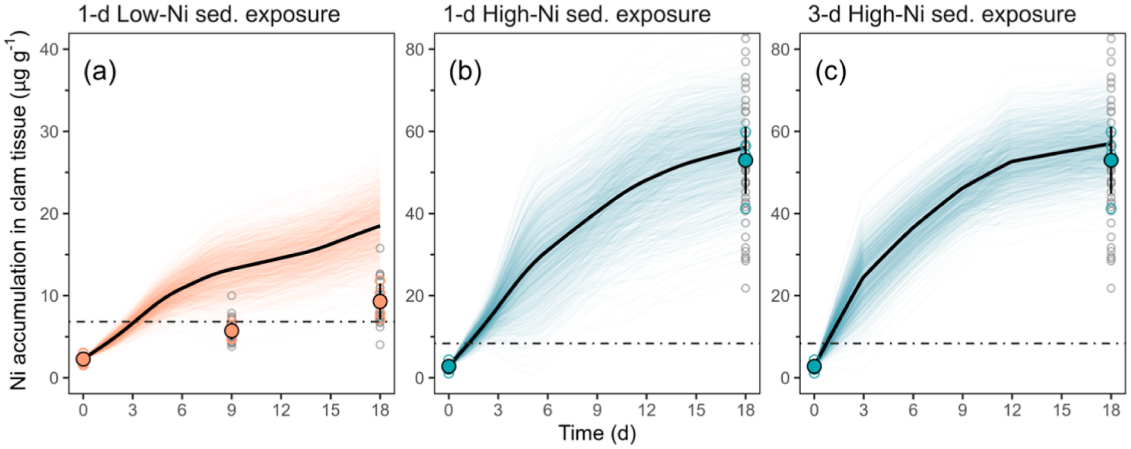

Figure 4. Biodynamic model with assimilation rates satisfactorily predicts the nickel accumulation in clam tissue. Note that the *y*-axis scale in panel (a) is smaller than that in panel (b,c). The color circles represent the average tissue nickel concentration of all clams within a replicate sediment chamber, while the empty gray circles indicate the tissue nickel concentrations of individual clams. The solid color points and the error bars represent the mean and standard deviation of tissue nickel concentrations of four replicate treatments, respectively. The curves are the predicted tissue nickel concentrations (thin curves, n = 1000; bold black curves: average). The horizontal dot−dash lines indicate three times the background clam tissue nickel concentration.

concentration. The dynamic fluctuation in nickel concentrations in both the overlying water and sediment, influenced by frequent water renewal and bioturbation activities, suggests that nickel in the system exists in a nonequilibrium state. This nonequilibrium condition may potentially result in temporal variations in nickel bioavailability over time.

3.3. Rapid Determination of Metal Bioavailability by the Isotopically Modified Bioassay. The 14 day isotopic modification process effectively altered the Ni isotopic composition in the clam assay, resulting in the accumulation of 0.26−0.64 μg g^{-1} of Ni^{62} in the clam tissues (Figure S6). Except for the second batch of modification, each independent batch of the modification operation produced similar levels of Ni^{62} accumulation. The second batch had a moderately higher accumulation of Ni^{62}, with a value of 0.64 ± 0.31 μg g^{-1}, while that of the other five batches ranged from 0.26 ± 0.12 μg g^{-1} to 0.44 ± 0.18 μg g^{-1}. However, these differences were not reflected in the $Ni^{62/60}$ isotopic ratio as the $Ni^{62/60}$ isotopic ratio across different batches did not show significant variations (p = 0.33, ANOVA, Figure S6). Therefore, we concluded that the efficiency of the isotopic modification operations was consistent, and the slight difference across different batches would not affect our interpretation of the nickel bioavailability results.

Upon exposure to nickel-contaminated sediment, the clams assimilated nickel from the sediment−water system, leading to the expected reduction in the $Ni^{62/60}$ ratio in the isotopically modified clams (Figure 2). Compared to the baseline group, the extent of the decrease in the $Ni^{62/60}$ ratio indicates varying degrees of nickel assimilation. In the low-Ni treatment, a 1 day exposure to the sediment resulted in a 34 ± 5% decrease in the $Ni^{62/60}$ ratio (Figure 2). In the high-Ni treatment, a 1 day exposure resulted in a more substantial decrease in the ratio (57 ± 5%). Prolonged exposure to the sediment (3 day exposure) led to even greater assimilation of nickel, as evidenced by a 73 ± 4% decrease in the $Ni^{62/60}$ ratio.

The decline of the $Ni^{62/60}$ ratio was further quantified as the net assimilation rate (ng of Ni g^{-1} h^{-1}) in different exposure scenarios (Figure 3). In the low-Ni treatment, the nickel assimilation rate ranged from 35 ± 18 to 78 ± 19 ng g^{-1} h^{-1}. In contrast, in the high-Ni treatment, the nickel assimilation rate was approximately 3.3 times higher, ranging from 110 ±

https://doi.org/10.1021/acs.est.3c05914
Environ. Sci. Technol. 2023, 57, 19352−19362

20 to 240 ± 130 ng g^{-1} h^{-1} following 1 day exposure and from 96 ± 39 to 320 ± 90 ng g^{-1} h^{-1} following a 3 day exposure (Figure 3). It is worth noting that the assimilation rates in the 1 day and 3 day exposure scenarios were consistent (p = 0.93, pairwise t-test), and both exhibited an overall decreasing trend over time, demonstrating the robustness of the approach in interpreting the dynamics of nickel bioavailability in the sediment, despite differences in exposure duration. However, certain nickel assimilation rate values showed notable differences compared to others. Specifically, in the low-Ni treatment, the 1 day nickel assimilation rate on Day 3−4 was approximately twice as high as the rates measured at other times (Figure 3). In the high-Ni treatment, the 1 day nickel assimilation rate showed greater variability, and the 3 day nickel assimilation rate on Day 0−3 was higher and more variable. We believe that these differences may be attributed to an interruption operation that occurred on Day 1, involving sediment rehomogenization to place a mesh within the sediment (as described in Section 2.2). This operation could have substantially disrupted the sediment structure and altered the redox conditions, consequently leading to increased variability in nickel bioavailability.

3.4. Predicting the Long-Term Bioaccumulation Using the Nickel Assimilation Rates. The 18 day sediment exposure significantly increased the tissue Ni concentration in both treatments (p < 0.001, Welch's t-test). In the low-Ni treatment, the tissue Ni concentrations increased from 2.3 ± 0.6 μg g^{-1} on Day 0 to 5.7 ± 1.0 μg g^{-1} on Day 9 and then further to 9.3 ± 2.2 μg g^{-1} on Day 18. This corresponds to an average nickel accumulation rate of 16 ng g^{-1} h^{-1} (Figure 4a) and a 4-fold increase in the tissue Ni concentration over the 18 day period. Similarly, in the high-Ni treatment, the tissue Ni concentrations increased from 2.8 ± 1.0 to 53 ± 8 μg g^{-1} over the 18 day period. This corresponds to a much higher nickel accumulation rate of 116 ng g^{-1} h^{-1} (Figure 4b,c).

The mean Ni accumulation rates estimated from long-term Ni exposure measurement (16 and 120 ng g^{-1} h^{-1} in the two treatments) were consistent with the Ni assimilation rates determined by the more rapid isotopically modified bioassay (35−78 and 111−239 ng g^{-1} h^{-1}). Therefore, we used the assimilation rates to model the Ni accumulation process during the 18 day exposure.

The modeled Ni bioaccumulation curves (Figure 4) successfully reproduced the observed changes in tissue Ni concentration during the 18 day sediment exposure. In the low-Ni treatment, the modeled curves exhibited an approximately constant increase in tissue Ni concentrations throughout the experiment (Figure 4a). The predicted tissue nickel concentrations on Day 9 and 18 were slightly higher than the measured concentrations but still fell within a factor of 3 of the measured values (Table S4).

In the high-Ni treatment, models based on both the 1 day and 3 day nickel assimilation rates showed increasing tissue Ni concentrations over time, although the rate of increase gradually declined (Figure 4b,c). The predicted tissue nickel concentrations in both scenarios were in good agreement with the observed increase in tissue Ni concentration during the 18 day sediment exposure. Specifically, the predicted mean tissue Ni concentration on Day 18 was 1.06 and 1.08 times of the measured tissue Ni concentration for the 1 day and 3 day assimilation rate models, respectively (Table S4).

Furthermore, it is important to emphasize that in the high-Ni treatment, the modeled curves exhibited a rapid initial increase followed by a plateau during the later period (Figure 4b,c). This pattern was attributed to a decrease in Ni assimilation rates within the system (Figure 3b,c), rather than being regulated by efflux processes within the organism. The contribution of efflux Ni to the total accumulated tissue nickel concentration was relatively small (Figure S7). Therefore, this change highlights the significant influence of dynamic changes in the metal bioavailability within the sedimentary system on metal bioaccumulation. It also suggests that such effects may not be adequately captured by long-term bioaccumulation tests typically with lower temporal resolution.

3.5. Merits, Limitations, and Implications for Risk Assessment of Metal-Contaminated Sediments. Developing a kinetic model that accurately simulates the metal accumulation process poses a challenging yet intriguing task in ecotoxicology. However, this proves particularly difficult in the context of sediments, where dietary uptake and the contribution of different exposure pathways need to be appropriately modeled.

Efforts have been made to parametrize the process of the dietary uptake of metals in sediments to enhance prediction capabilities. The two commonly used variables for this purpose are sediment ingestion rate (IR) and assimilation efficiency (AE).[2,5] While carefully designed experiments have successfully quantified these parameters,[19] transferring them to other studies to predict metal bioaccumulation in different sediments has proven difficult. The bioavailability of metals in sediments can vary significantly depending on sediment composition factors such as particle size composition, redox conditions, content of binding phases.[14,17,18] Consequently, the parameters derived become not only species-specific but also sediment-specific, limiting their applicability for predicting metal bioaccumulation in the assessment of metal-contaminated sediments.

In this study, we compared the isotopically modified bioassay and the long-term bioaccumulation bioassay under identical exposure conditions. The results demonstrated that the directly measured assimilation rates, which are related to bioavailability, can accurately predict the long-term bioaccumulation process for the same species exposed to the same conditions. This approach eliminates the complexity associated with modeling metal uptake from various sources, thus simplifying the application of a biodynamic model for predicting metal bioaccumulation in the sedimentary environment. Consequently, this advancement represents a practical and streamlined alternative for assessing the metal bioavailability in sediments.

Metal internalization is often considered the initial step in the cascade of toxicity, where an excessive tissue burden of metals surpasses an organism's regulatory capacity for excretion or detoxification, leading to the manifestation of toxicity effects. Models integrating metal bioaccumulation and toxicity development processes are commonly employed to assess the risk of metal exposure. Examples include the toxicokinetic−toxicodynamic model (TKTD) used mostly in water. The biodynamic model, utilizing metal assimilation rates as an input variable, can be readily integrated within these models to quantify the internalization of metals and to predict the effects of metal exposure.

The biodynamic modeling approach developed in this study offers valuable insights into the metal accumulation kinetics. This approach not only enables us to estimate the time required for a "magnitude" increase in tissue concentration (as

https://doi.org/10.1021/acs.est.3c05914
Environ. Sci. Technol. 2023, 57, 19352−19362

shown in Figure 4, with 4 days in the low-Ni treatment and 1 day in the high-Ni treatment for a 3-fold increase) but also opens up possibilities for assessing tissue metal concentrations in relation to potential toxicity thresholds. While this capability allows for an exploration of the potential toxicity risk associated with sediment exposure, it is important to acknowledge that any definitive assessment of toxicity would require additional considerations, such as critical body burden values or other relevant toxicity metrics. Effectively, the metal assimilation rate measurement may provide insights into the "dose rate" that could potentially contribute to metal toxicity. By considering the uptake and loss kinetics, the biodynamic model contributes to our understanding of the relationship between bioaccumulation and potential toxicity for metal contaminants, suggesting avenues for further investigation and risk assessment in sediment management.

While our bioaccumulation study yielded promising results in a controlled laboratory environment, where we examined two distinct levels of nickel-contaminated sediments prepared in the laboratory, extending this approach to predict nickel or other metal bioaccumulation under real-world conditions remains untested and requires comprehensive validation. This validation process may involve the use of field-collected sediment cores or direct field applications, encompassing additional complexities. Nonetheless, the inherent adaptability of the isotopically modified bioassay holds promise for addressing this challenge.

Although in this study we spiked Ni into clean sediments to investigate bioaccumulation, such an operation is not obligatory. The significant advantage of the isotopically modified bioassay is that sediment labeling is not needed, allowing for the assessment of metal bioavailability in its original speciation within the sediment.[22−25] This feature makes the isotopically modified bioassay highly amenable for examining naturally contaminated sediments, whether in a laboratory or field setting, offering valuable insights for environmental risk assessment and management.

Furthermore, our investigation entailed the preparation of two nickel concentrations in sediment: one representing a moderately contaminated scenario and the other representing a heavily contaminated scenario. The original intent of the study was to examine the toxicity to the survival of the clams when exposed to the heavily contaminated sediment. Surprisingly, despite clams accumulating tissue Ni concentrations exceeding 50 $\mu g\ g^{-1}$ by the end of the sedimentary bioaccumulation test, their survival remained unimpaired. This unexpected resilience suggests a high tolerance of this particular clam species to nickel contamination. To further enhance the applicability of this method, especially when targeting the assessment of toxicity risks in contaminated sediment, future studies could explore the use of more sensitive species to evaluate both bioaccumulation and toxicity effects.

In conclusion, this study demonstrates the successful integration of nickel assimilation rates determined using the isotopically modified bioassay into a biodynamic model for predicting nickel bioaccumulation. By streamlining the approach and eliminating the need to differentiate metal uptake from various pathways, this method becomes a reliable tool for predicting metal bioaccumulation in contaminated sediments. Furthermore, the potential for integration into a toxicity-informed model, such as the TKTD, offers promising prospects for linking bioaccumulation with metal toxicity risks in sedimentary environments. This advancement holds significant value in aiding informed decision-making in ecological risk assessment and management, contributing to a more comprehensive understanding of the risks associated with metal-contaminated sediments.

■ ASSOCIATED CONTENT

Supporting Information

The Supporting Information is available free of charge at https://pubs.acs.org/doi/10.1021/acs.est.3c05914.

Details on the DGT application and analysis, sampling and analysis, aqueous exposure-depuration test to determine the nickel efflux rate constant, sediment characterization results, Fe and Mn concentrations in overlying water and determined by DGTs, concentrations of newly accumulated Ni62, and the corresponding isotopic Ni62/60 ratios at the end of the isotopic-modification stage across different batches (PDF)

■ AUTHOR INFORMATION

Corresponding Author

Minwei Xie − *State Key Laboratory of Marine Environmental Science, Key Laboratory of the Ministry of Education for Coastal and Wetland Ecosystem, College of the Environment and Ecology, Xiamen University, Xiamen 361102 Fujian, China;* orcid.org/0000-0003-4359-8738; Email: minweixie@xmu.edu.cn

Authors

Qijing Su − *State Key Laboratory of Marine Environmental Science, Key Laboratory of the Ministry of Education for Coastal and Wetland Ecosystem, College of the Environment and Ecology, Xiamen University, Xiamen 361102 Fujian, China*

Wenze Xiao − *State Key Laboratory of Marine Environmental Science, Key Laboratory of the Ministry of Education for Coastal and Wetland Ecosystem, College of the Environment and Ecology, Xiamen University, Xiamen 361102 Fujian, China*

Stuart L. Simpson − *Centre for Environmental Contaminants Research, CSIRO Environment, Sydney 2334 New South Wales, Australia; Southern Marine Science and Engineering Guangdong Laboratory, Guangzhou 511458 Guangdong, China*

Qiao-Guo Tan − *State Key Laboratory of Marine Environmental Science, Key Laboratory of the Ministry of Education for Coastal and Wetland Ecosystem, College of the Environment and Ecology, Xiamen University, Xiamen 361102 Fujian, China;* orcid.org/0000-0001-9692-6622

Rong Chen − *State Key Laboratory of Marine Environmental Science, Key Laboratory of the Ministry of Education for Coastal and Wetland Ecosystem, College of the Environment and Ecology, Xiamen University, Xiamen 361102 Fujian, China*

Complete contact information is available at: https://pubs.acs.org/10.1021/acs.est.3c05914

Notes

The authors declare no competing financial interest.

https://doi.org/10.1021/acs.est.3c05914
Environ. Sci. Technol. 2023, 57, 19352−19362

■ ACKNOWLEDGMENTS

We express our gratitude to Haiyan Xiong and Zeting Yu for their assistance during the conduction of the experiment. We thank the three anonymous reviewers for their constructive comments to improve this paper. This study was supported by the National Natural Science Foundation of China (grant no. 42077372) and the Hong Kong Branch of Southern Marine Science and Engineering Guangdong Laboratory (gno. SMSEGL20SC02).

■ REFERENCES

(1) Van der Oost, R.; Beyer, J.; Vermeulen, N. P. Fish bioaccumulation and biomarkers in environmental risk assessment: a review. *Environ. Toxicol. Pharmacol.* **2003**, *13* (2), 57−149.
(2) Luoma, S. N.; Rainbow, P. S. *Metal Contamination in Aquatic Environments: Science and Lateral Management*; Cambridge University Press, 2008.
(3) Pan, K.; Wang, W. X. Trace metal contamination in estuarine and coastal environments in China. *Sci. Total Environ.* **2012**, *421*−*422* (3), 3−16.
(4) Santos-Echeandía, J.; Campillo, J. A.; Egea, J. A.; Guitart, C.; González, C. J.; Martínez-Gómez, C.; León, V. M.; Rodríguez-Puente, C.; Benedicto, J. The influence of natural vs anthropogenic factors on trace metal (loid) levels in the Mussel Watch programme: Two decades of monitoring in the Spanish Mediterranean sea. *Mar. Environ. Res.* **2021**, *169*, 105382.
(5) Luoma, S. N.; Rainbow, P. S. Why is metal bioaccumulation so variable? Biodynamics as a unifying concept. *Environ. Sci. Technol.* **2005**, *39* (7), 1921−1931.
(6) Rainbow, P. S. Trace metal bioaccumulation: models, metabolic availability and toxicity. *Environ. Int.* **2007**, *33* (4), 576−582.
(7) Campana, O.; Taylor, A. M.; Blasco, J.; Maher, W. A.; Simpson, S. L. Importance of subcellular metal partitioning and kinetics to predicting sublethal effects of copper in two deposit-feeding organisms. *Environ. Sci. Technol.* **2015**, *49* (3), 1806−1814.
(8) Adams, W. J.; Blust, R.; Borgmann, U.; Brix, K. V.; DeForest, D. K.; Green, A. S.; Meyer, J. S.; McGeer, J. C.; Paquin, P. R.; Rainbow, P. S.; et al. Utility of tissue residues for predicting effects of metals on aquatic organisms. *Integr. Environ. Assess. Manage.* **2011**, *7* (1), 75−98.
(9) Simpson, S.; Batley, G. *Sediment Quality Assessment: A Practical Guide*; CSIRO Publishing: Melbourne, Victoria, Australia, 2016.
(10) Wang, W.-X. Incorporating exposure into aquatic toxicological studies: an imperative. *Aquat. Toxicol.* **2011**, *105* (3−4), 9−15.
(11) Wang, W.-X.; Fisher, N. S.; Luoma, S. N. Kinetic determinations of trace element bioaccumulation in the mussel Mytilus edulis. *Mar. Ecol.: Prog. Ser.* **1996**, *140*, 91−113.
(12) Tan, Q.-G.; Wang, W.-X. Two-compartment toxicokinetic-toxicodynamic model to predict metal toxicity in Daphnia magna. *Environ. Sci. Technol.* **2012**, *46* (17), 9709−9715.
(13) Tan, Q.-G.; Lu, S.; Chen, R.; Peng, J. Making acute tests more ecologically relevant: cadmium bioaccumulation and toxicity in an estuarine clam under various salinities modeled in a toxicokinetic-toxicodynamic framework. *Environ. Sci. Technol.* **2019**, *53* (5), 2873−2880.
(14) Simpson, S. L.; Batley, G. E. Predicting metal toxicity in sediments: a critique of current approaches. *Integr. Environ. Assess. Manage.* **2007**, *3* (1), 18−31.
(15) Lee, B.-G.; Griscom, S. B.; Lee, J.-S.; Choi, H. J.; Koh, C.-H.; Luoma, S. N.; Fisher, N. S. Influences of dietary uptake and reactive sulfides on metal bioavailability from aquatic sediments. *Science* **2000**, *287* (5451), 282−284.
(16) Luoma, S.; Fisher, N. Uncertainties in assessing contaminant exposure from sediments. In *Ecological Risk Assessment of Contaminated Sediments*; Dillon, T., Biddinger, G. R., Eds.; SETAC Press: Pensacola, FL, 1996; pp 211−237.
(17) Eggleton, J.; Thomas, K. V. A review of factors affecting the release and bioavailability of contaminants during sediment disturbance events. *Environ. Int.* **2004**, *30* (7), 973−980.
(18) Chapman, P. M.; Wang, F.; Janssen, C.; Persoone, G.; Allen, H. E. Ecotoxicology of metals in aquatic sediments: binding and release, bioavailability, risk assessment, and remediation. *Can. J. Fish. Aquat. Sci.* **1998**, *55* (10), 2221−2243.
(19) Wang, W.-X.; Fisher, N. S. Assimilation efficiencies of chemical contaminants in aquatic invertebrates: A synthesis. *Environ. Toxicol. Chem.* **1999**, *18* (9), 2034−2045.
(20) Fan, W.; Wang, W. X. Sediment geochemical controls on Cd, Cr, and Zn assimilation by the clam Ruditapes philippinarum. *Environ. Toxicol. Chem.* **2001**, *20* (10), 2309−2317.
(21) King, C. K.; Simpson, S. L.; Smith, S. V.; Stauber, J. L.; Batley, G. E. Short-term accumulation of Cd and Cu from water, sediment and algae by the amphipod Melita plumulosa and the bivalve Tellina deltoidalis. *Mar. Ecol.: Prog. Ser.* **2005**, *287*, 177−188.
(22) Croteau, M. N.; Cain, D. J.; Fuller, C. C. Novel and nontraditional use of stable isotope tracers to study metal bioavailability from natural particles. *Environ. Sci. Technol.* **2013**, *47* (7), 3424−3431.
(23) Croteau, M. N.; Cain, D. J.; Fuller, C. C. Assessing the dietary bioavailability of metals associated with natural particles: extending the use of the reverse labeling approach to zinc. *Environ. Sci. Technol.* **2017**, *51* (5), 2803−2810.
(24) Wu, Q.; Zheng, T.; Simpson, S. L.; Tan, Q.-G.; Chen, R.; Xie, M. Application of a multi-metal stable-isotope-enriched bioassay to assess changes to metal bioavailability in suspended sediments. *Environ. Sci. Technol.* **2021**, *55* (19), 13005−13013.
(25) Wu, Q.; Su, Q.; Simpson, S. L.; Tan, Q.-G.; Chen, R.; Xie, M. Isotopically modified bioassay bridges the bioavailability and toxicity risk assessment of metals in bedded sediments. *Environ. Sci. Technol.* **2022**, *56* (23), 16919−16928.
(26) Vieira, S.; Barrulas, P.; Chainho, P.; Dias, C. B.; Sroczyńska, K.; Adão, H. Spatial and temporal distribution of the multi-element signatures of the estuarine non-indigenous bivalve Ruditapes philippinarum. *Biol. Trace Elem. Res.* **2022**, *200*, 385−401.
(27) Kanaya, G.; Nobata, E.; Toya, T.; Kikuchi, E. Effects of different feeding habits of three bivalve species on sediment characteristics and benthic diatom abundance. *Mar. Ecol.: Prog. Ser.* **2005**, *299*, 67−78.
(28) Ji, C.; Cao, L.; Li, F. Toxicological evaluation of two pedigrees of clam Ruditapes philippinarum as bioindicators of heavy metal contaminants using metabolomics. *Environ. Toxicol. Pharmacol.* **2015**, *39* (2), 545−554.
(29) Gillmore, M. L.; Price, G. A. V.; Golding, L. A.; Stauber, J. L.; Adams, M. S.; Simpson, S. L.; Smith, R. E. W.; Jolley, D. F. The diffusive gradients in thin films (DGT) technique predicts nickel toxicity to the amphipod *Melita plumulosa*. *Environ. Toxicol. Chem.* **2021**, *40*, 1266−1278.
(30) Wang, Z.; Yeung, K. W.; Zhou, G.-J.; Yung, M. M.; Schlekat, C. E.; Garman, E. R.; Gissi, F.; Stauber, J. L.; Middleton, E. T.; Lin Wang, Y. Y.; et al. Acute and chronic toxicity of nickel on freshwater and marine tropical aquatic organisms. *Ecotoxicol. Environ. Saf.* **2020**, *206*, 111373.
(31) Mudd, G. M. Global trends and environmental issues in nickel mining: Sulfides versus laterites. *Ore Geol. Rev.* **2010**, *38* (1−2), 9−26.
(32) Fernandez, J.-M.; Ouillon, S.; Chevillon, C.; Douillet, P.; Fichez, R.; Gendre, R. L. A combined modelling and geochemical study of the fate of terrigenous inputs from mixed natural and mining sources in a coral reef lagoon (New Caledonia). *Mar. Pollut. Bull.* **2006**, *52* (3), 320−331.
(33) Noël, V.; Morin, G.; Juillot, F.; Marchand, C.; Brest, J.; Bargar, J. R.; Muñoz, M.; Marakovic, G.; Ardo, S.; Brown, G. E. Ni cycling in mangrove sediments from New Caledonia. *Geochim. Cosmochim. Acta* **2015**, *169*, 82−98.
(34) Simpson, S. L.; Angel, B. M.; Jolley, D. F. Metal equilibration in laboratory-contaminated (spiked) sediments used for the develop-

https://doi.org/10.1021/acs.est.3c05914
Environ. Sci. Technol. 2023, 57, 19352−19362

ment of whole-sediment toxicity tests. *Chemosphere* **2004**, *54* (5), 597−609.
(35) Lewis, M.; Pryor, R.; Wilking, L. Fate and effects of anthropogenic chemicals in mangrove ecosystems: a review. *Environ. Pollut.* **2011**, *159* (10), 2328−2346.
(36) Birch, G.; Lee, J.-H.; Tanner, E.; Fortune, J.; Munksgaard, N.; Whitehead, J.; Coughanowr, C.; Agius, J.; Chrispijn, J.; Taylor, U.; et al. Sediment metal enrichment and ecological risk assessment of ten ports and estuaries in the World Harbours Project. *Mar. Pollut. Bull.* **2020**, *155*, 111129.
(37) Costello, D. M.; Burton, G. A.; Hammerschmidt, C. R.; Rogevich, E. C.; Schlekat, C. E. Nickel phase partitioning and toxicity in field-deployed sediments. *Environ. Sci. Technol.* **2011**, *45* (13), 5798−5805.
(38) Davison, W.; Zhang, H. Progress in understanding the use of diffusive gradients in thin films (DGT)-back to basics. *Environ. Chem.* **2012**, *9* (1), 1−13.
(39) Davison, W. *Diffusive Gradients in Thin-Films for Environmental Measurements*; Cambridge University Press: Cambridge, 2016.
(40) Xie, M.; Simpson, S. L.; Huang, J.; Teasdale, P. R.; Wang, W.-X. In Situ DGT sensing of bioavailable metal fluxes to improve toxicity predictions for sediments. *Environ. Sci. Technol.* **2021**, *55* (11), 7355−7364.
(41) United States Environmental Protection Agency. *Method 3051A (SW-846). Microwave Assisted Acid Digestion of Sediments, Sludges, Soils, and Oils*: Washington, DC, 2007.

https://doi.org/10.1021/acs.est.3c05914
Environ. Sci. Technol. 2023, 57, 19352−19362

Enhancing Sediment Bioaccumulation Predictions: Isotopically-modified Bioassay and Biodynamic Modeling for Nickel Assessment

Supporting Information

Qijing Su[1], Wenze Xiao[1], Stuart L. Simpson[2,3], Qiao-Guo Tan[1], Rong Chen[1], Minwei Xie[1,*]

1. State Key Laboratory of Marine Environmental Science, Key Laboratory of the Ministry of Education for Coastal and Wetland Ecosystem, College of the Environment and Ecology, Xiamen University, Xiamen 361102, Fujian, China
2. Centre for Environmental Contaminants Research, CSIRO Environment, Sydney 2334, New South Wales, Australia
3. Southern Marine Science and Engineering Guangdong Laboratory, Guangzhou 511458, Guangdong, China

*Corresponding Author: minweixie@xmu.edu.cn

This supporting information material consists 13 pages, including 4 tables and 7 figures.

Figure S1. Tagging of the unmodified clams for identification. A plastic tag was securely attached to the clam shell using glue, ensuring it remained in place throughout the experiment, even during movement within the sediment. A ruler with centimeter scale was used for size measurement.

S1. DGT application and data analysis

Piston DGT samplers (DGT® Research Ltd.) were deployed to measure labile metal concentrations in the sediments. These samplers consist of a piston-type plastic holder that houses three layers: a filter membrane, a porous diffusive gel layer, and a Chelex-100 resin binding layer.[1] This type of passive sampler was originally designed to measure dissolved metal concentrations in surface water.[1] Recently, it has been adapted for sediment applications to measure labile metal concentrations in the porewater and those loosely bound to sediment particles.[2-4]

Prior to being deployed in the sediment, the DGT samplers were deoxygenated in 0.05 M NaCl solution for approximately 2 h. The DGT pistons were then vertically inserted into the sediment until their upper rim level with the sediment water interface (SWI).[50] This placement provided a measurement of labile metals at the depth of 0.5–2.5 cm below the SWI (exposure area = 3.14 cm^2). Following a 24-h deployment, the DGT samplers were retrieved, rinsed with deionized water to remove attached sediments, transferred into a clean zip bag, and stored at 4℃ until analysis.

As part of the quality control, an additional 4 blank DGT samplers underwent the same operational procedures but were not deployed in the sediment.

Within 40 days of DGT retrieval, the deployed and blank DGT samplers were disassembled. The metal-binding layer of each sampler was then digested in 1 mL of 1 M HNO_3 for 24 h. Following the digestion, the eluent was further diluted with

deionized water and submitted to the inductively coupled plasma mass spectrometry instrument (ICP-MS, NexION 2000, PerkinElmer) to determine the concentrations of Fe, Mn and Ni.

The measured metal concentrations in the eluent were then converted to the time-weighted average concentration of labile metal (C_{DGT}) using the equation $C_{DGT} = M \cdot \Delta g/(D \cdot t \cdot A)$, where M is the mass of metal accumulated in the binding gel layer (ng), Δg is the total thickness of diffusive gel layer and the filter membrane (cm), D is the diffusion coefficient of metals in the diffusive layer ($cm^2\ s^{-1}$), t is the deployment time (s) and A is the exposure area (A=3.14 cm^2).

Assuming a 24-h deployment, the background metal concentrations of the blank DGT samplers were < 0.03 μg L^{-1} for Ni, < 0.2 μg L^{-1} for Mn, and < 2 μg L^{-1} for Fe, all of which were substantially lower than the labile metal concentrations found in deployed DGT samplers. The labile metal concentrations measured in all deployed DGT samplers were thus corrected by subtracting the mean concentrations measured in the blank DGT samplers.

It is important to note that the concentration measured by the DGT device (C_{DGT}) may not always equal the porewater metal concentration. The correspondence between C_{DGT} and porewater concentration depends on the resupply conditions of metals from the solid phase to the porewater during DGT deployment.[5, 6]

In cases where metals are rapidly resupplied from the solid phase for the entire deployment period, C_{DGT} approximates the bulk porewater concentration. Conversely, in situations with no resupply or partial resupply (and potentially slowing with time), C_{DGT} is lower than the porewater metal concentration.

Studies have suggested that, for metals such as Fe and Mn, resupply is fully sustained, while for others like Ni, it is only partially sustained.[5] For simplicity, we have referred to these concentrations as DGT-labile concentrations in sediments without specifying whether C_{DGT} equals porewater metal concentrations for each metal.

S2. Sampling and analysis

Sediments were characterized for basic properties, including the particle size distribution, the dilute-acid extractable metals (AEM) and the total recoverable metal (TRM) concentration. The field collected clean sediment was successively sieved through two meshes with pore sizes of 150 μm and 75 μm, resulting in the identification of three sediment size fractions. The AEM content of the clean and Ni-spiked sediment was determined by adding 0.5 g wet homogenized sediments in 20 mL 1 M HCl and extracting for 1 h.[7] The TRM content of both sediments was determined following the U.S. EPA. Method 3051A,[8] by extracting 0.5 g dry sediments in 9 mL 65% nitric acid for 20 min at 180°C within a microwave digestion system (Milestone ETHOS UP, Italy).

Over the course of bioaccumulation experiment, overlying seawater was sampled on Day 0, 1, 3, 4, 6, 7, 9, 10, 12, 13, 15, 16 and 18, both before and after the water renewal. Ten mL of the overlying water was filtered using a PES membrane filter with a pore size of 0.45 μm. The filtered seawater was acidified to a pH < 1 with HNO_3, and stored at room temperature. These filtered seawater samples were further diluted 10 times before being submitted to the ICP-MS instrument.

The clam samples from the water culture and the sediment were processed immediately following retrieval. To terminate metal uptake, these clams were immersed immediately into 1 mM EDTA solution for 1 min. Subsequently, the clams were dissected using a stainless-steel scalpel. The soft tissue of the clams was rinsed sequentially with the EDTA solution and deionized water, stored in clean zip bags at -20 °C, and freeze-dried before digestion. Dried tissue samples (0.035~0.13 g) were first cold-digested at room temperature overnight in 1 mL of 65% HNO_3, and then hot digested at 80 °C for 8 h. The acid digest solution samples were then diluted and submitted to the ICP-MS to determine concentrations of different metal isotopes.

Metal concentrations in water and acid digest were determined by ICP-MS. For nickel, Ni^{60} and Ni^{62} was analyzed. Mn and Fe in the DGT eluent samples were also analyzed. During the analysis, an internal reference standard of 5 μg L^{-1} Ge^{74} was also monitored and used to correct the influence of potential instrumental shift and matrix effects. Samples with known concentrations were determined every 15-20 samples to

test the reproducibility of analysis. As an overall quality control for the digestion of organism tissue and sediment, as well as the subsequent instrumental analysis, the metal concentrations in the certified reference material (oyster tissue SRM 1566b and marine sediment MESS-4) were determined using identical procedures. The recovery of TRM-Ni was 98 ± 1% (n = 3) for the organism tissue, whereas it was lower at 73 ± 1% (n =3) for sediment samples. This reduced recovery of total nickel concentration in the reference sediment material can be attributed to the presence of nickel within a recalcitrant fraction, making it resistant to extraction by concentrated nitric acid during the digestion process. In contrast, the spiked nickel in the sediment is more likely to be loosely bound to the sediment grains, resulting in a closer alignment between the determined TRM-Ni concentrations in spiked sediments and their nominal values.

S3. Supplementary aqueous exposure-depuration test to determine the nickel efflux rate constant

The determination of the nickel efflux rate constant involved conducting a supplementary aqueous exposure-depuration test. During this test, the clams were exposed to Ni^{62}-spiked seawater for a period of 2 days, followed by a depuration in clean seawater for an additional 26 days.

During the exposure phase, to maintain a constant concentration of Ni^{62} (5 μg L^{-1}), the clams were placed in a flow-through chamber containing 6.6 L of Ni^{62}-spiked seawater, providing 60 mL of water per clam. The water renewal rate was controlled at 1.3 mL min^{-1}, resulting in a turnover time of 1 day. Throughout the 2-d exposure stage, the clams were not fed.

After the 2-d exposure, the clams were transferred to a static-renewal system, where clean seawater was provided with daily water renewal (60 mL water per clam). During the subsequent 26-d depuration stage, the clams were fed with the green algae Chlorella sp. at a rate of 3.5 mg per clam for 1 h in a separate container, which occurred every two days before the water renewal.

To monitor the changes in the accumulated concentration of Ni^{62} in clam tissue,

six clams were randomly sampled from the system at specific time intervals: 0, 3, 7, 12, and 24 h on the first day, and 2, 2.5, 3, 4, 6, 9, 12, 16, 22, and 28 days thereafter. These sampled clams were treated and subjected to Ni isotope analysis in the clam tissue using the same procedures described in the main text (Section 2.6.1).

The change of newly accumulated Ni^{62} concentration ($Ni^{62}|_{new}$) in the clam tissue is shown in Figure S2. During the 2-d exposure phase, $Ni^{62}|_{new}$ displayed a linear increase over time. In the subsequent 26-d depuration phase, $Ni^{62}|_{new}$ demonstrated an initial rapid decrease, which then transitioned into a slower decline. This observed pattern suggests that a two-compartment biodynamic model is suitable for describing the processes of aqueous uptake and elimination of nickel within the clam.[9, 10]

The two-compartment biodynamic model conceptualizes two metal-storage pools within an organism, namely C_1 and C_2, as illustrated in Figure S3. These two pools correspond to a fast-exchange pool and a slow-exchange pool, respectively.[10, 11] In the fast-exchange pool, nickel is readily exchanged with the surrounding ambient water and can also serve as a source of nickel for the slow-exchange pool. On the other hand, nickel stored in the slow-exchange pool can be directly eliminated into the ambient water. To account for the growth dilution effect, the model also includes a growth rate constant.

$$C(t) = C_1(t) + C_2(t) \quad \text{(S1)}$$

$$\frac{dC_1(t)}{dt} = k_u \cdot C_w(t) - (k_{e1} + k_{12} + g) \cdot C_1(t) \quad \text{(S2)}$$

$$\frac{dC_2(t)}{dt} = k_{12} \cdot C_1(t) - k_{e2} \cdot C_2(t) \quad \text{(S3)}$$

where $C(t)$, $C_1(t)$, and $C_2(t)$ represent the concentration of nickel stored in the clam tissue, in the fast-exchange pool, and in the slow-exchange pool, respectively (μg g^{-1}). $C_w(t)$ represents the concentration of Ni^{62} spiked in the seawater (μg L^{-1}). The variable k_u is the uptake rate constant (L g^{-1} d^{-1}), and k_{e1} and k_{e2} are the elimination rate constant (d^{-1}) of nickel from the fast-exchange and the slow-exchange pool, respectively. The rate constant k_{12} (d^{-1}) represents the transfer of nickel from the fast-exchange pool to the slow-exchange pool. The parameter g corresponds to the growth rate constant of the clam (d^{-1}) and was determined based on the average rate of change

in the dry weight of the clam tissue during the test.

The model parameters (k_u, k_{e1}, k_{e2}, and k_{12}) were simultaneously fitted by applying equations S1-S3 to the accumulated Ni^{62} in clam tissue throughout the uptake and depuration stage. The software OpenModel (version 2.4.2), developed by Nei Crout at Nottingham University, was employed to estimate the best-fit values and uncertainties using the Marquardt algorithm.[12] The resulting best-fit curve was visualized using the "ggplot2" package in R (version 4.2.2) (Figure S2).

In the development of the biodynamic model (equation 8-10 in the main text) for clams exposed to the sedimentary environment, the nickel efflux process was also included and we assume that the clams exhibit the same efflux rate constant in sediments as they do in water. As a result, the rate constant k_{e2} from above was adapted and referred to as k'_e in equation 9. This adjustment was made to reflect the significance of the slow-exchange pool in dictating the long-term loss of metals.

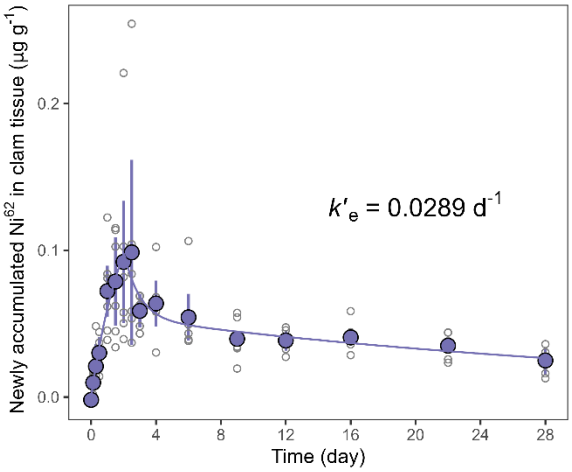

Figure S2. Concentration of newly accumulated Ni^{62} ($Ni^{62}|_{new}$) in the clams during the 2-d exposure stage followed by a 26-d depuration. The solid points and the error bars represent the mean and the standard deviation of $Ni^{62}|_{new}$ for a group of individual clams (indicated by grey circles). The curve represents the best-fit of the mean $Ni^{62}|_{new}$ using the biodynamic model.

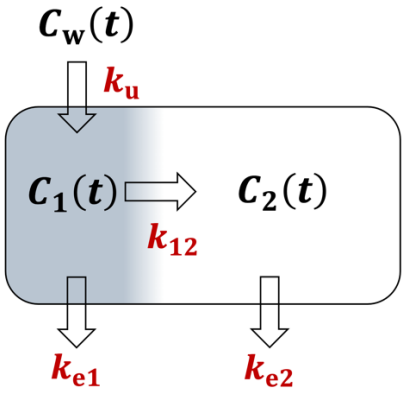

Figure S3. Conceptualization of the two-compartment biodynamic model depicting nickel uptake and elimination in clams exposed to Ni-spiked seawater. The model incorporates two compartments representing fast-exchanging (C_1) and slow-exchanging (C_2) pools. For parameter definitions, refer to equations S1-S3.

Table S1. Parameters of the biodynamic model for clams exposed to Ni-spiked seawater. Values of the parameters are mean ± standard deviation.

Parameters	Value
k_u (L g^{-1} d^{-1})	0.016 ± 0.001
k_{e1} (d^{-1})	0.70 ± 0.07
$k'_e = k_{e2}$ (d^{-1})	0.029 ± 0.003
k_{12} (d^{-1})	0.35 ± 0.03
g (d^{-1})	-0.0016

Table S2. Metal concentrations in clean sediment

	Metal	Background Concentrations	SQGVs†
AEM (mg kg^{-1} dry weight) n=3	Ni	3.3 ± 1.4	21
	Cd	0.12 ± 0.05	1.5
	Cu	6.1 ± 0.5	65
	Pb	24 ± 2	50
	Zn	39 ± 3	200
	Fe	4900 ± 300	-
	Mn	390 ± 20	-
TRM (mg kg^{-1} dry weight) n=3	Ni	23 ± 1	21
	Cd	0.14 ± 0.01	1.5
	Cu	21 ± 2	65
	Pb	47 ± 3	50

	Zn	120 ± 10	200
	Fe	41000 ± 2000	-
	Mn	830 ± 10	-
Particle size distribution (Mass fraction)	>150 µm	4.5%	-
	75-150 µm	2.9%	-
	<75 µm	92.6%	-

†SQGVs = lower sediment quality guideline values.[7]

Table S3. Nickel concentrations in nickel-spiked sediment

	Low-Ni treatment	**High-Ni treatment**
AEM-Ni (n=12) (mg kg^{-1} dry weight)	210 ± 40	1700 ± 100
TRM-Ni (n = 4) (mg kg^{-1} dry weight)	260 ± 10	2300 ± 200
mean_AEM-Ni/mean_TRM-Ni	81%	74%
$C_{DGT\text{-}Ni}$ (n=18) † (µg L^{-1})	87 ± 23	1200 ± 740
K_d ‡ (L kg^{-1})	3000	1900
log K_d (L kg^{-1})	3.48	3.28

† DGT-labile Ni concentrations measured during the bioaccumulation experiment

‡ The partition coefficient was K_d estimated by dividing mean of TRM-Ni to the mean porewater Ni concentration represented by the $C_{DGT\text{-}Ni}$

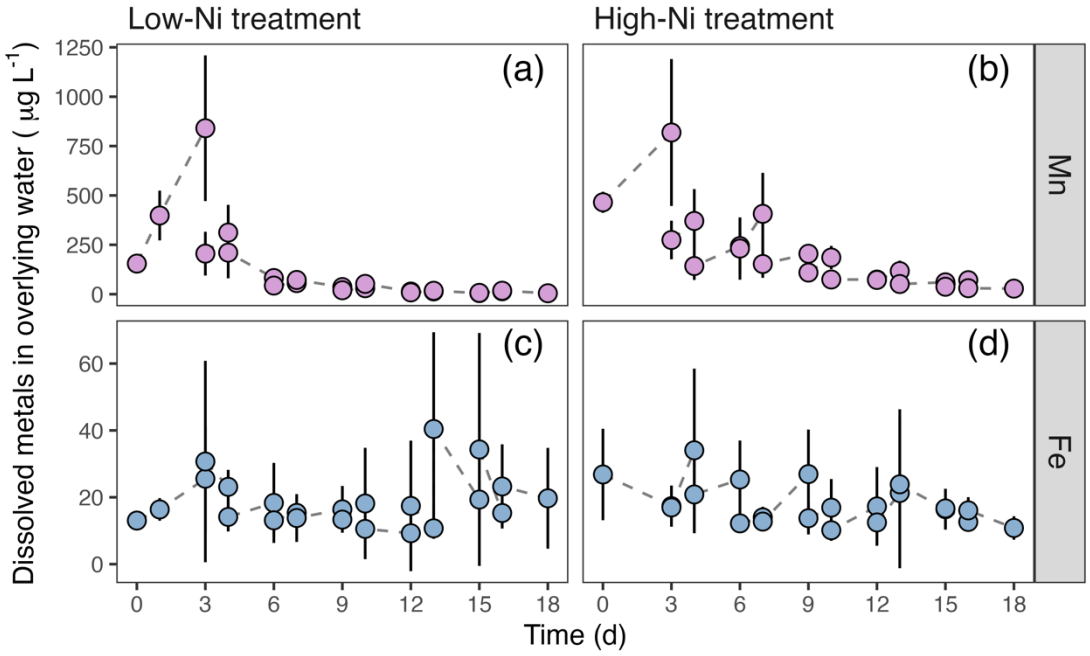

Figure S4. Dissolved Fe and Mn concentrations in the overlying water in different Ni-spiked sediments. The solid point and the error bar represent the mean and the standard deviation of dissolved metal concentrations in the overlying water of the four replicate chambers.

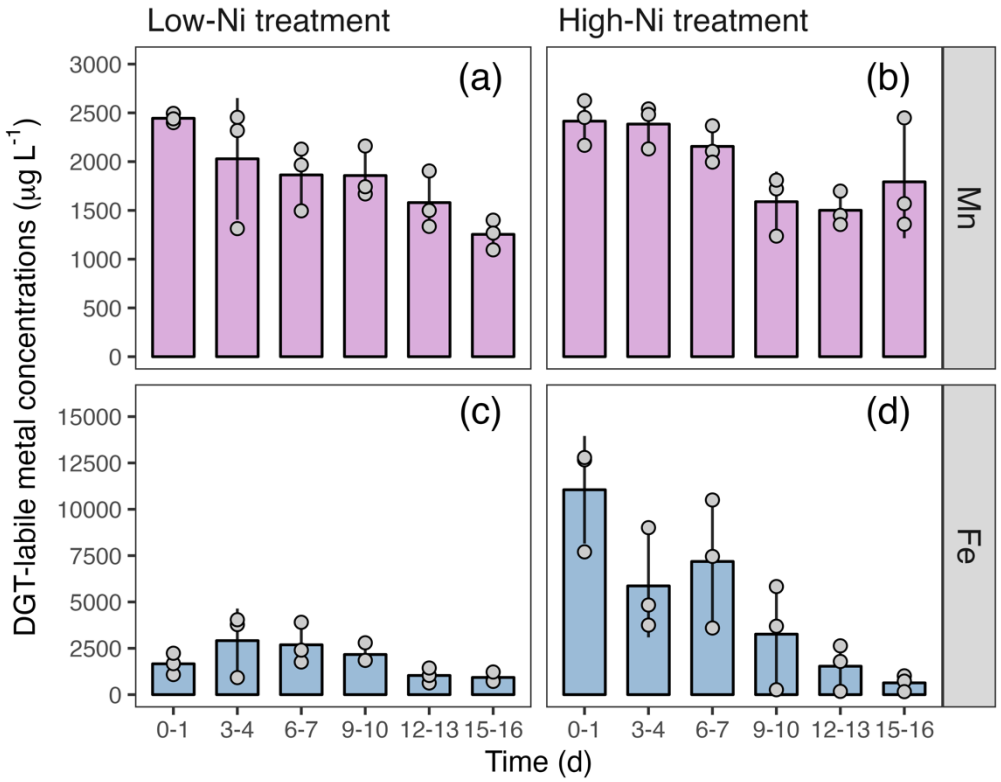

Figure S5. DGT-labile Fe and Mn concentrations in different Ni-spiked sediments. Each gray solid point represents a measurement in a replicate treatment. The height of each column and the error bar represent the mean and the standard deviation of three replicates.

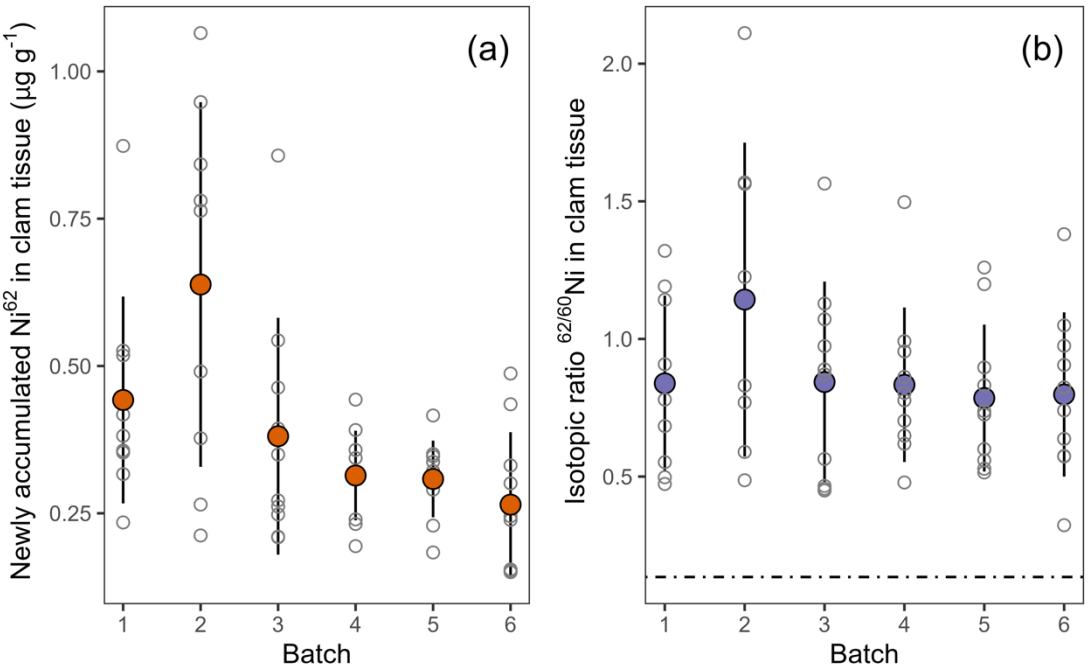

Figure S6. Concentrations of newly accumulated Ni^{62} (a) and the corresponding isotopic ratio $Ni^{62/60}$ in clam tissue at the end of the 14-d isotopic-modification stage across six batches. The Ni^{62}-spiked seawater concentration was 5 μg L^{-1}, and six batch of clams were cultured separately in the spiked seawater for 14 days. (a) Each open circle represents the concentration of newly accumulated Ni^{62} in an individual clam, the solid points depict the mean, and the error bars indicate standard deviations. (b) Each open circle represents the isotopic ratio $Ni^{62/60}$ of an individual clam, the solid points show the mean, and the error bars represent the standard deviations. The horizontal dot-dashed line indicates the $Ni^{62/60}$ isotopic ratio of unmodified clams.

Table S4. The measured and model predicted mean concentrations of Ni in clam tissue

Treatment	**Time** (day)	**Measured** (μg g^{-1})	**Predicted** (μg g^{-1})	**Factor** (Predicted/Measured)
1-d Low-Ni sed. exposure	0	2.3	2.3	-
	9	5.8	13	2.31
	18	9.3	18	1.99
1-d High-Ni sed. exposure	0	2.8	2.8	-
	18	53	56	1.06
3-d High-Ni sed. exposure	0	2.8	2.8	-
	18	53	57	1.08

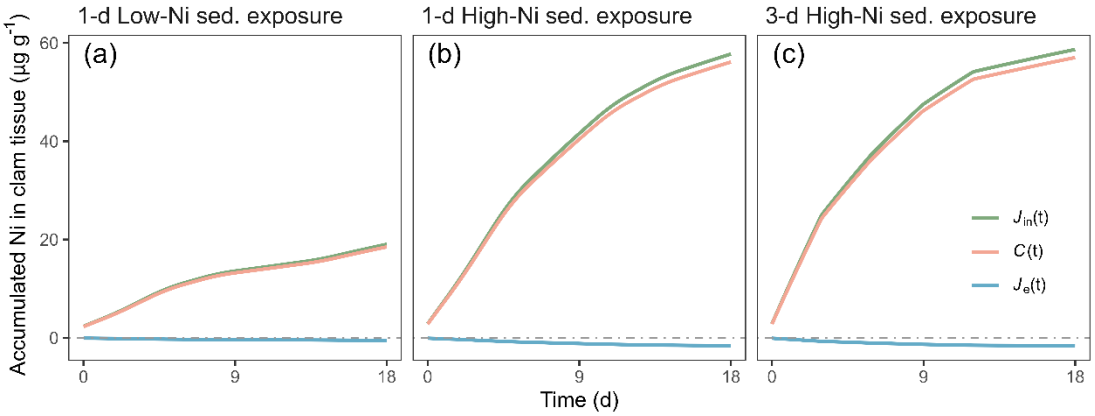

Figure S7. Relative contribution of metal influx and efflux processes to the modeled nickel tissue concentrations. Refer to Equation 8 in the main text for explanation of the symbols.

References:

1. Davison, W.; Zhang, H., In situ speciation measurements of trace components in natural waters using thin-film gels. *Nature* **1994,** *367*, (6463), 546-548.

2. Gillmore, M. L., Price, G.A.V., Golding, L.A., Stauber, J.L., Adams, M.S., Simpson, S.L., Smith, R.E.W., Jolley, D.J., The diffusive gradients in thin films (DGT) technique predicts nickel toxicity to the amphipod *Melita plumulosa*. *Environmental Toxicology and Chemistry* **2020,** *40*, 1266-1278.

3. Zhang, Y.; Yang, J.; Simpson, S. L.; Wang, Y.; Zhu, L., Application of diffusive gradients in thin films (DGT) and simultaneously extracted metals (SEM) for evaluating bioavailability of metal contaminants in the sediments of Taihu Lake, China. *Ecotoxicology and Environmental Safety* **2019,** *184*, 109627.

4. Xie, M.; Simpson, S. L.; Huang, J.; Teasdale, P. R.; Wang, W.-X., In Situ DGT sensing of bioavailable metal fluxes to improve toxicity predictions for sediments. *Environmental Science & Technology* **2021,** *55*, (11), 7355-7364.

5. Zhang, H.; Davison, W.; Mortimer, R. J.; Krom, M. D.; Hayes, P. J.; Davies, I. M., Localised remobilization of metals in a marine sediment. *Science of the Total Environment* **2002,** *296*, (1), 175-187.

6. Zhang, H.; Davison, W.; Miller, S.; Tych, W., In situ high resolution measurements of fluxes of Ni, Cu, Fe, and Mn and concentrations of Zn and Cd in porewaters by DGT. *Geochimica et Cosmochimica Acta* **1995,** *59*, (20), 4181-4192

7. Simpson, S.; Batley, G., *Sediment quality assessment: a practical guide*. CSIRO Publishing: Melbourne, Victoria, Australia, 2016.

8. EPA., U. S. *Method 3051A (SW-846). Microwave assisted acid digestion of sediments, sludges, soils, and oils*; Washington, DC, 2007.

9. Rainbow, P.; Luoma, S., Metal toxicity, uptake and bioaccumulation in aquatic invertebrates—modelling zinc in crustaceans. *Aquatic toxicology* **2011,** *105*, (3-4), 455-465.

10. Tan, Q.-G.; Wang, W.-X., Two-compartment toxicokinetic–toxicodynamic model to predict metal toxicity in Daphnia magna. *Environmental science & technology* **2012,** *46*, (17), 9709-9715.

11. Chen, W.-Q.; Wang, W.-X.; Tan, Q.-G., Revealing the complex effects of salinity on copper toxicity in an estuarine clam Potamocorbula laevis with a toxicokinetic-toxicodynamic model. *Environmental Pollution* **2017,** *222*, 323-330.

12. Tan, Q.-G.; Zhou, W.; Wang, W.-X., Modeling the toxicokinetics of multiplem metals in the oyster *Crassostrea hongkongensis* in a dynamic estuarine environment. *Environmental Science & Technology* **2018,** *52*, (2), 484-492.